# Regulation of osteoclast function and bone mass by RAGE

Zheng Zhou,[1] David Immel,[2] Cai-Xia Xi,[1] Angelika Bierhaus,[3] Xu Feng,[4] Lin Mei,[1] Peter Nawroth,[3] David M. Stern,[5] and Wen-Cheng Xiong[1]

[1]Institute of Molecular Medicine and Genomics and Department of Neurology, Medical College of Georgia, Augusta, GA, 30912
[2]Savannah River National Laboratory, Aiken, SC 29808
[3]Department of Medicine I, University of Heidelberg, 69120 Heidelberg, Germany
[4]Department of Pathology, University of Alabama at Birmingham, Birmingham, AL 35294
[5]Dean's Office, College of Medicine, University of Cincinnati, Cincinnati, OH 45267

**The receptor for advanced glycation end products (RAGE) is a member of the immunoglobulin superfamily that has multiple ligands and is implicated in the pathogenesis of various diseases, including diabetic complications, neurodegenerative disorders, and inflammatory responses. However, the role of RAGE in normal physiology is largely undefined. Here, we present evidence for a role of RAGE in osteoclast maturation and function, which has consequences for bone remodeling. Mice lacking RAGE had increased bone mass and bone mineral density and decreased bone resorptive activity in vivo. In vitro–differentiated RAGE-deficient osteoclasts exhibited disrupted actin ring and sealing zone structures, impaired maturation, and reduced bone resorptive activity. Impaired signaling downstream of $\alpha_v\beta_3$ integrin was observed in RAGE$^{-/-}$ bone marrow macrophages and precursors of OCs. These results demonstrate a role for RAGE in osteoclast actin cytoskeletal reorganization, adhesion, and function, and suggest that the osteosclerotic-like phenotype observed in RAGE knockout mice is due to a defect in osteoclast function.**

CORRESPONDENCE
Wen-Cheng Xiong:
wxiong@mcg.edu

Abbreviations used: BMD, bone mineral density; BMM, bone marrow macrophage; BV, bone volume; HMGB, high mobility group box; M-CSF, macrophage colony-stimulating factor; MMP9, matrix metaloproteinase 9; μCT, microcomputer tomographic; pre-OC, preosteoclast; Pyd, deoxypyridinoline; RAGE, receptor for advanced glycation end products; RANKL, receptor activator of NF-κB ligand; ROS, reactive oxygen species; TRAP, tartrate-resistant acid phosphatase; TREM, triggering receptors expressed by myeloid cells; TV, tissue volume; VN, vitronectin.

Osteoclasts are multinucleated, terminally differentiated cells from hematopoietic monocyte/macrophage precursors responsible for bone resorption (degradation of mineralized matrix), a critical event regulating bone mass. Osteoclast differentiation is regulated by multiple factors, including macrophage colony-stimulating factor (M-CSF) and receptor activator of NF-κB ligand (RANKL; also known as ODF and TRANCE) (1–4). Recently, triggering receptors expressed by myeloid cells (TREM)2, a receptor of the immunoglobulin superfamily, DC-STAMP, a putative seven-transmembrane receptor, and possible other RANK-independent receptors have been implicated in osteoclast differentiation (5–11). Osteoclast activation is initiated upon cell attachment to bone matrix, an event leading to osteoclast actin cytoskeletal reorganization and formation of sealing zones and a polarized ruffled membrane (12). When osteoclasts are cultured on glass surfaces, unique cell adhesion structures, called podosomes and/or actin rings, are formed. They are related to, but distinct from, the typical focal adhesions formed in cultured fibroblasts or epithelial cells. Podosomes consist of a core of F-actin bundles surrounded by a rosette-like structure containing integrins (e.g., $\alpha_v\beta_3$) and actin-binding proteins, such as α-actinin and gelsolin (13–15). In addition, signaling molecules are enriched at podosomes/actin rings, including tyrosine kinases (c-Src and PYK2 [13, 16–18]), adaptor-like proteins ($p130^{Cas}$ [Crk-associated substrate; 19] and Cbl [a negative regulator of multiple tyrosine kinases; 20, 21]), phosphatidylinositol-3 kinase (22), and rho family G proteins (23). Thus, stimulation of the $\alpha_v\beta_3$ integrin by cell attachment to bone matrix (e.g., vitronectin) elicits a series of biochemical responses, including activation of cytoplasmic tyrosine kinases, such as Src and PYK2, and subsequent tyrosine phosphorylation of several proteins including Cbl and $p130^{Cas}$. These signaling molecules are essential for osteoclast actin cytoskeletal organization and function.

RAGE, a member of the immunoglobin superfamily of cell surface receptors, has been implicated in the pathogenesis of multiple

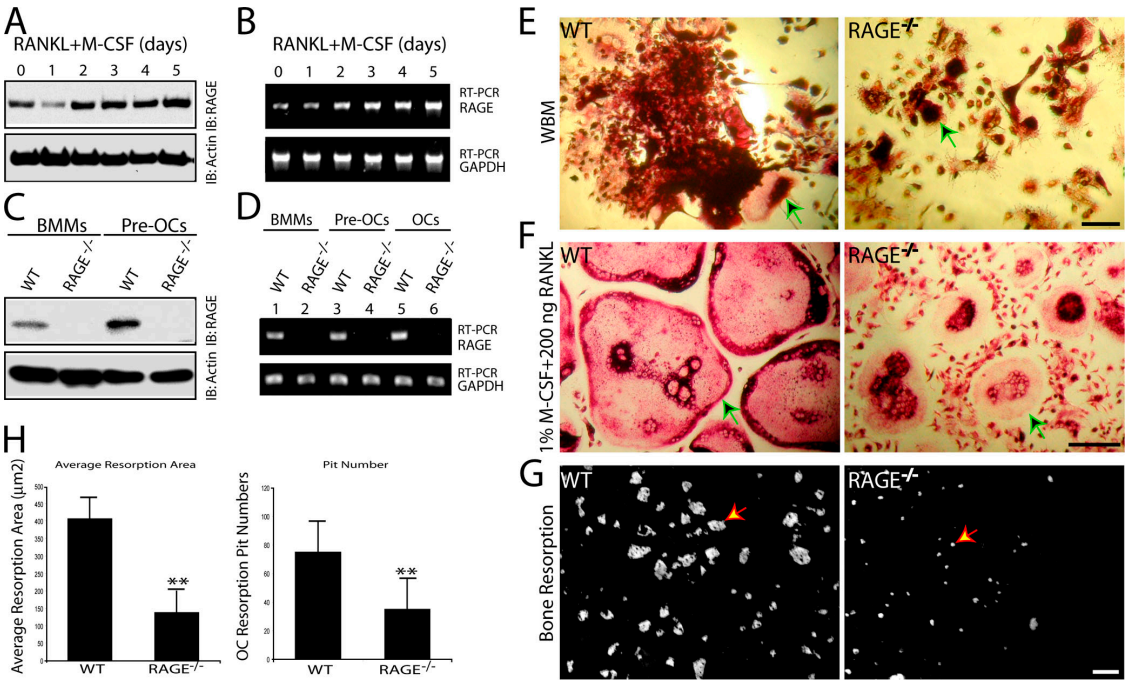


**Figure 1. Morphologic and functional defects of in vitro–differentiated RAGE mutant OCs.** RAGE expression in BMMs and differentiating osteoclasts (OCs) derived from WT and RAGE$^{-/-}$ mice was examined by Western blot analysis (A and C) and RT-PCR (B and D). In A and B, purified BMMs from WT mice were incubated with M-CSF (10%) for 2–3 d and then cultured in the presence of RANKL (100 ng/ml) and M-CSF (1%) for 0–5 d, as indicated. In C and D, pre-OCs and osteoclasts were generated from purified BMMs cultured in the presence of RANKL (100 ng/ml) and M-CSF (1%) for 2 and 4 d, respectively (see Materials and methods). In E, osteoclasts were generated from whole bone marrow (WBM) in the presence of 1,25(OH) vitamin D3 (see Materials and methods), and in F, osteoclasts were generated from purified BMMs cultured in the presence of RANKL (100 ng/ml) and M-CSF (1%) for 7 d. Morphologic characteristics of WT and RAGE$^{-/-}$ osteoclasts were determined by TRAP staining (E and F). Representative bone resorption caused by WT and RAGE$^{-/-}$ osteoclasts was visualized by Von Kossa staining (G). The bone resorption assay was performed by culturing osteoclasts on coverslips coated with calcium phosphate matrix for 8 d, and then staining coverslips with Von Kossa to display resorption pits (white) (see Materials and methods). Quantitative analysis of the average resorption area and pit number based on data from G is shown in H. **, $P < 0.01$, significant difference from the WT (Student's *t* test). Green arrows in E and F indicate DCs, and red arrows in G indicate resorptive pits. Bars, 50 μm.

disorders, including diabetic complications (24, 25), neurodegeneration (26), and inflammatory conditions (27). The link between RAGE and these pathological situations is the multiligand character of the receptor and its ability to sustain cellular activation (28). Ligands of RAGE include diabetes-associated advanced glycation end products (24, 25), Alzheimer's disease-associated amyloid β-peptide (26) and proinflammatory-associated Mac-1/β2 integrin (29), the S100 family, and high mobility group box (HMGB)1 (30). HMGB1, also called amphoterin or HMG1, is a nuclear protein released from activated macrophages or injured cells (31). Once in the extracellular space, HMGB1 displays proinflammatory cytokine-like properties (31). Although the possible contribution of RAGE to pathologic states has been studied, the role of this receptor in homeostatic/physiologic settings has yet to be elucidated. Several lines of evidence suggest a role for RAGE in immune/inflammatory responses, beyond its capacity to bind proinflammatory cytokines (32). For example, RAGE is involved in the recruitment of inflammatory cells to activated endothelium (33–35). Engagement of endothelial RAGE increases expression of vascular cell adhesion molecule-1, intercellular adhesion molecule-1, and endothelial cell selectin, and enhances adhesion of inflammatory cells, such as neutrophils and monocytes, to stimulated endothelia (33–35). In addition, RAGE expression by activated endothelia promotes leukocyte recruitment, via its interaction with myeloid cells expressing the $\beta_2$ integrin macrophage receptor 1 (29). Furthermore, studies using RAGE-deficient mice have shown the receptor to be important in innate immunity (32, 36). In sepsis induced by cecal ligation and puncture, a model largely dependent on the innate immune response, RAGE-deficient mice exhibit increased survival, which correlated with reduced local inflammation and decreased NF-κB activation in target organs of septic shock (36). Such a protective phenotype in RAGE-null animals in response to sepsis was reversed by restoring RAGE expression in hematopoietic and endothelial cells, suggesting an intrinsic role of RAGE in these cells. Among hematopoietic cells, macrophages have a key role in innate immunity and inflammation (36). However, the contribution of RAGE to macrophage differentiation and activation remains to be fully elucidated.

Here, we identify RAGE as an essential factor in the regulation of osteoclast maturation and function. Using gene-targeted mice, we show that RAGE deficiency leads to morphologically and functionally disrupted osteoclasts and an osteopetrosis-like phenotype. In addition, we provide evidence for impaired osteoclast terminal differentiation and reduced integrin-mediated cell adhesion signaling in bone marrow macrophages (BMMs) and prefusion osteoclasts (pre-OCs) derived from RAGE mutant mice. These results suggest a novel role of RAGE in osteoclast maturation/function and bone remodeling. In addition, our findings provide insight into a mechanism for regulation of cell adhesion by RAGE and imply a conserved function of RAGE in cells of monocyte/macrophage lineage.

## RESULTS

### Morphological and functional defects of in vitro–differentiated RAGE$^{-/-}$ osteoclasts

RAGE is highly expressed in hematopoietic cells, including BMMs (Fig. 1, A and B). Its expression detected by Western blot and RT-PCR analyses appeared to be up-regulated during osteoclast differentiation (Fig. 1, A and B). However, the role of RAGE in osteoclast differentiation and function is unclear. To address this question, in vitro osteoclastogenesis was examined using cultures of whole bone marrow cells derived from WT and RAGE-deficient (RAGE$^{-/-}$) mice under osteoclastogenic conditions, in which stromal cells (precursors of osteoblasts) provide M-CSF and RANKL, two essential factors for osteoclast development (1–4). BMMs derived from RAGE$^{-/-}$ mice showed undetectable RAGE expression (Fig. 1, C and D), confirming the presence of a null allele in the mutant mouse (37). It is of interest to note that BMMs differentiated from RAGE$^{-/-}$ bone marrow cultures appeared smaller in size compared with cells from WT cultures, although they were positive for tartrate-resistant acid phosphatase (TRAP), a marker of the osteoclast differentiation (Fig. 1 E). These results suggest a morphologic defect in in vitro–differentiated RAGE$^{-/-}$ osteoclasts, which could reside in stromal cells that failed to produce sufficient amounts of M-CSF and/or RANKL or in osteoclastic precursors (e.g., macrophages).

Thus, we examined whether RAGE deficiency impaired the capacity of osteoclastic precursors to respond to M-CSF

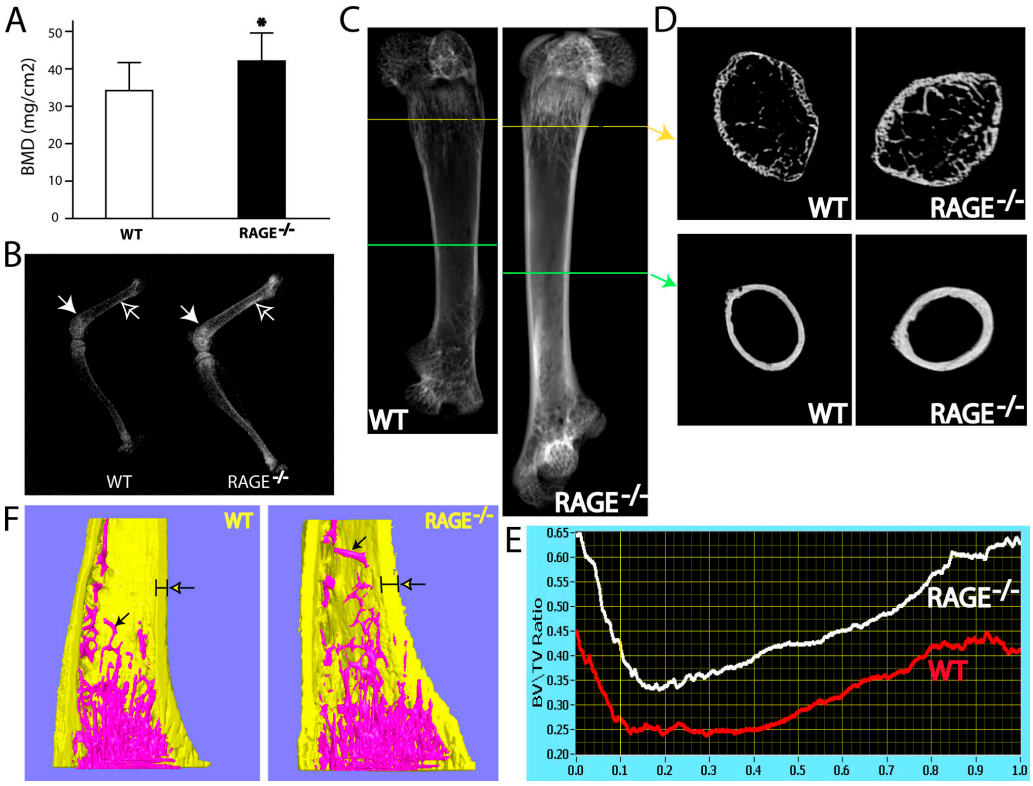


**Figure 2. Increased bone mass in 4-wk-old RAGE$^{-/-}$ mice.** (A) Pixus densitometric analysis of the BMD of whole bone mass from 4-wk-old WT and RAGE$^{-/-}$ mice. Increased BMD was observed in RAGE$^{-/-}$ mice. (B) Radiographic analysis of 4-wk-old WT and RAGE$^{-/-}$ mice. Femurs and tibiae from RAGE$^{-/-}$ mice show increased density of both cortical (empty arrows) and trabecular (filled arrows) bones. (C) μ-CT images of femurs isolated from control C57BL/6 (WT) and RAGE$^{-/-}$ mice. Note that an increased bone length and increased trabecular and cortical bone mass were observed. The cross section images corresponding to the indicated position (yellow and green lines) were shown in D. Quantitative analysis of the ratio of BV/TV at the different positions of femurs from WT and RAGE$^{-/-}$ was shown in E. Three-dimensional images of tibia isolated from WT and RAGE$^{-/-}$ mice were shown in F. Increased cortical (yellow) and trabecular (purple) bone mass was indicated. (A and F) *, $P < 0.05$, significant difference from WT (Student's *t* test).

and/or RANKL in vitro. To this end, purified BMMs from WT and RAGE$^{-/-}$ mice were exposed to M-CSF and RANKL for 7 d to induce osteoclastic differentiation. Cultures of WT BMMs formed confluent sheets of large TRAP-positive cells, and >80% of these cells displayed typical spread, multinucleated characteristics of in vitro–differentiated osteoclasts (Fig. 1 F). However, RAGE$^{-/-}$ cultures, although rich in BMMs, contained only smaller, poorly spread, but TRAP-positive multinucleated cells (Fig. 1 F). Only ~20% of the multinucleated cell population displayed spread morphology, consistent with the defect of in vitro osteoclastogenesis observed in cultures of whole bone marrow cells. As this experiment was performed using purified BMMs, the osteoclastogenic defect in RAGE$^{-/-}$ whole marrow cultures may reside in osteoclast precursors, but not in cytokine-producing stromal cells. In addition to the morphologic defects of in vitro–differentiated osteoclasts, RAGE$^{-/-}$ TRAP-positive cells exhibited functional defects in bone resorption with significantly reduced numbers and average sizes of pits (Fig. 1, G and H). Collectively, these results indicate that RAGE deficiency leads to generation of morphologically and functionally impaired osteoclasts, suggesting a role for RAGE in regulating osteoclastic differentiation and function in vitro.

### Defects of osteoclast function in RAGE$^{-/-}$ mice

We next determined whether RAGE regulates osteoclast differentiation and function in vivo by examining bone mass in RAGE$^{-/-}$ mice, as osteoclasts play a critical role in maintenance of healthy bone. Pixus densitometric analysis showed a significant increase in bone mineral density (BMD) of whole bones in 4-wk-old RAGE$^{-/-}$ mice compared with that of age- and strain-matched WT mice (Fig. 2 A), suggesting an increase of bone mass in RAGE mutant mice. The latter possibility was further supported by radiographic (Fig. 2 B) and microcomputer tomographic (μCT) analyses. 4-wk-old RAGE$^{-/-}$ mice displayed an increase in the density of trabecular and cortical bone area in femurs and tibia (Fig. 2, C–F). These results implicate a defect of osteoclast function in RAGE$^{-/-}$ mice. To test this concept, serum deoxypyridinoline (Pyd), an indicator of bone resorption (collagen matrix degradation) in vivo, was measured in WT and RAGE$^{-/-}$ mice. Indeed, Pyd in sera of RAGE$^{-/-}$ mice was significantly reduced (Fig. 3 A) compared with that in WT mice, confirming a role for RAGE in regulating osteoclast function in vivo.

These results led us to evaluate the possible involvement of RAGE in osteoclast differentiation in vivo by histological examination of WT and RAGE$^{-/-}$ femur and tibia. The number of osteoclasts per unit bone volume (unpublished data) and the total number of osteoclasts per unit resorptive surface was reduced in RAGE$^{-/-}$ tibia and femurs (Fig. 3 D). Consistent with impaired function of osteoclasts in RAGE$^{-/-}$ mice, bone volume (over the total volume, or the total bone volume) was increased in femur from these animals (Fig. 3, B–C and E). Based on these observations, we propose that RAGE contributes to osteoclast function in vivo.

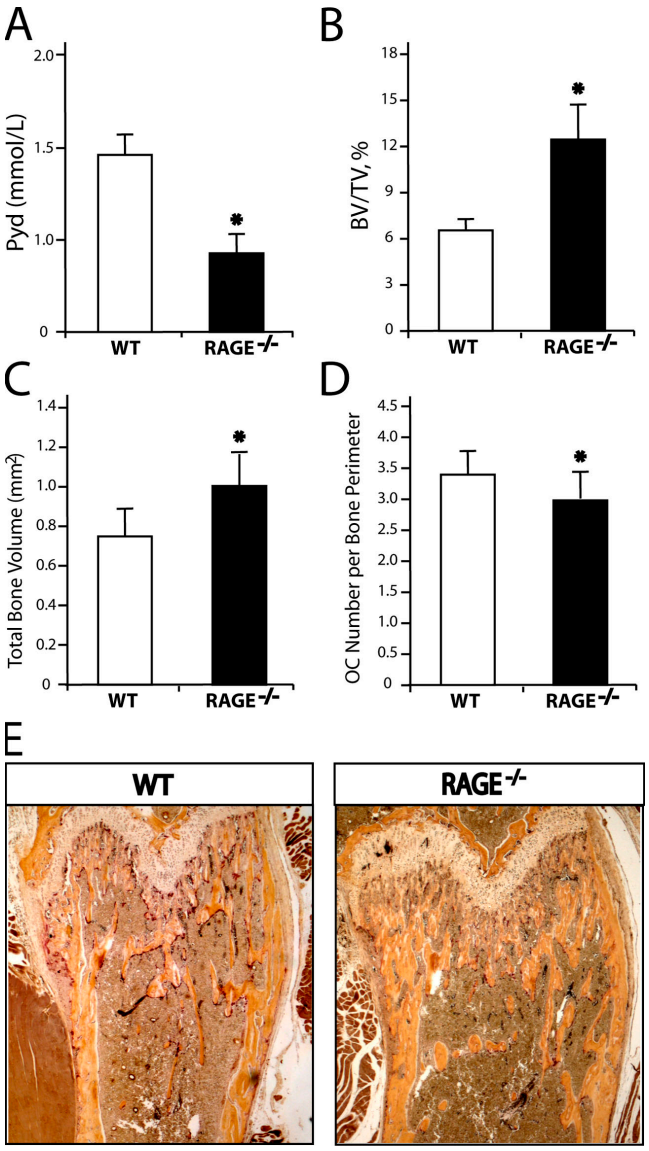


**Figure 3. Decreased bone resorptive activity and increased bone volume in RAGE$^{-/-}$ mice.** (A) Measurement of serum Pyd levels in WT and RAGE$^{-/-}$ mice by ELISA. (B and C) Quantitative analysis of trabecular bone of WT and RAGE$^{-/-}$ mice expressed as the percentage of trabecular bone volume versus total marrow space (BV/TV) (B) or as total bone volume (C). $n = 3$. (A–D) * $P < 0.05$, significant difference from WT (Student's $t$ test). (D) Quantitative analysis of the number of osteoclasts in WT and RAGE$^{-/-}$ tibia and femurs expressed as total osteoclast number per bone resorptive surface (mm) (fields counted per each slide = 5, $n = 3$). (E) Histomorphologic analysis of sections of femurs from 4-wk-old WT and RAGE$^{-/-}$ mice. Histologic sections of femurs were stained for TRAP activity (purple) to identify OCs and counterstained with methyl green to visualize cortical thickness and trabecular mass.

### Defective $\alpha_v\beta_3$-dependent signaling in RAGE$^{-/-}$ BMMs and pre-OCs

Impaired osteoclastogenesis in vitro led us to examine whether M-CSF and/or RANKL signaling in RAGE$^{-/-}$ BMMs was altered. M-CSF and its receptor, c-Fms, drive

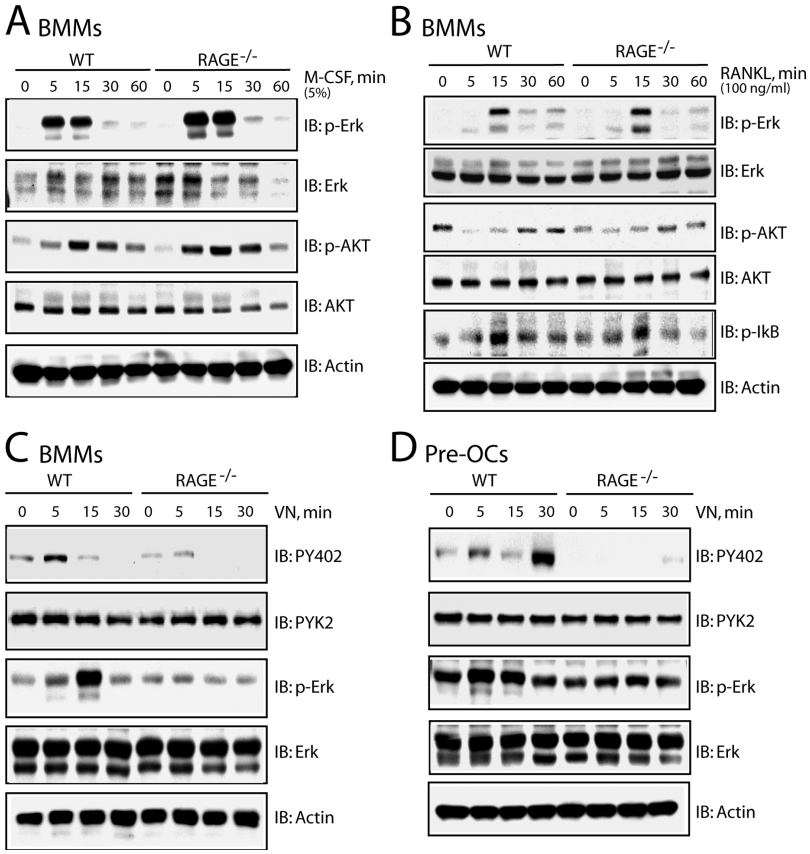


**Figure 4. Defective $\alpha_v\beta_3$-dependent signaling in RAGE$^{-/-}$ BMMs and pre-OCs.** M-CSF (A) and RANKL (B) signaling in BMMs derived from WT and RAGE$^{-/-}$ mice were studied by Western blot analysis of the phosphorylated p42/p44 form of Erk (p-Erk), AKT (p-AKT), or IκB (p-IκB) at the indicated times. Levels of total Erk, AKT, or β-actin were used as controls for protein loading. In C and D, VN-stimulated signaling was determined by Western blot analysis for the presence of phosphorylated tyrosine at residue 402 in PYK2 (PY402) and phosphorylated Erk (p-Erk). Total PYK2, Erk, or β-actin levels were used as loading controls. BMMs (C) and pre-OCs (D) derived from WT and RAGE$^{-/-}$ mice were lifted and replated onto VN-coated dishes for the indicated times or left in suspension (0 min).

early lineage development from BMMs and are essential for osteoclastic survival (2). WT and RAGE$^{-/-}$ BMMs proliferated equally in response to M-CSF (unpublished data), suggesting the absence of a defect in the early stage of the response of RAGE$^{-/-}$ BMMs to M-CSF. Indeed, M-CSF–induced phosphorylation of extracellular signal–regulated kinase (Erk1)/2 and AKT/PKB (protein kinase B) was normal in RAGE$^{-/-}$ BMMs (Fig. 4 A). We then examined RANKL signaling responses in RAGE$^{-/-}$ BMMs. RANKL and its receptor, RANK, are essential for the development of BMMs to mature osteoclasts (3, 4). RANKL activation of NF-κB and Erk1/2 is required for efficient osteoclastogenesis (1). Notably, RANKL-driven phosphorylation of Erk1/2 and Akt (Fig. 4 B) and RANKL-induced activation of NF-κB, assessed by IκB-α phosphorylation (Fig. 4 B) and nuclear translocation of p65 (unpublished data), appeared to be normal in RAGE$^{-/-}$ BMMs. These results suggest that RAGE has no or little effect on M-CSF– or RANKL-induced early signaling events in BMMs.

We next examined whether $\alpha_v\beta_3$-mediated signaling was impaired in RAGE$^{-/-}$ BMMs and pre-OCs, as integrin $\alpha_v\beta_3$-mediated cell adhesion plays an essential role in osteoclastic maturation and function (12). WT or RAGE$^{-/-}$ BMMs and pre-OCs were plated on dishes coated with vitronectin (VN), a ligand for $\alpha_v\beta_3$. Tyrosine phosphorylation of PYK2 (PY402) and phosphorylation of Erk1/2 were examined, as they are "activated" by engagement of integrin $\alpha_v\beta_3$ in BMMs and pre-OCs (Figs. 4, C and D). Remarkably, these signaling events were attenuated or blocked in RAGE$^{-/-}$ BMMs or pre-OCs (Figs. 4, C and D), demonstrating an impairment of $\alpha_v\beta_3$-mediated signaling in RAGE$^{-/-}$ cells. Moreover, this event appeared to be specific, since M-CSF–induced Src and Erk phosphorylation were unaffected in RAGE$^{-/-}$ BMMs (Fig. 4 and unpublished data). Collectively, these results suggest a critical role of RAGE in regulating integrin- (i.e., $\alpha_v\beta_3$) mediated signaling in osteoclast precursors.

### Defects of actin cytoskeletal organization and terminal differentiation in in vitro–cultured RAGE$^{-/-}$ osteoclasts

Integrin engagement leads to actin cytoskeletal reorganization and formation of actin rings and podosomes in

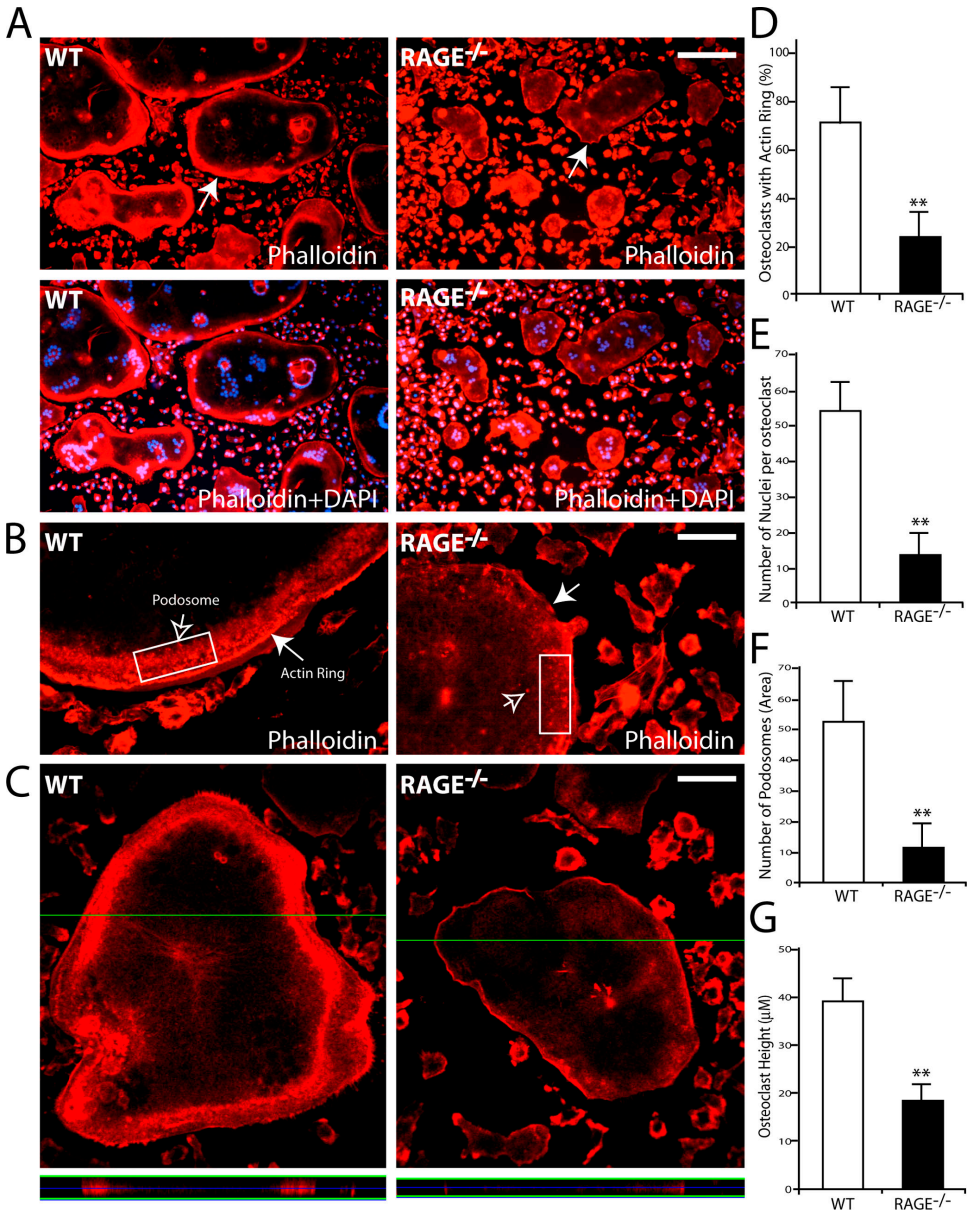


**Figure 5. Defects of actin-based cytoskeletal organization in RAGE$^{-/-}$ osteoclasts.** Osteoclasts differentiated from BMMs of WT and RAGE$^{-/-}$ mice were cultured on glass and visualized with phalloidin (for the actin cytoskeleton) and DAPI (for nuclei). A shows lower magnification images, and B and C show higher magnification images. The arrows in A and B indicate OCs. The quantitative areas are indicated by rectangular boxes in B. The green horizontal lines in C indicate the positions of z axis for the measurement of the heights of OCs. (D) Quantification of the percentage of osteoclasts with intact actin ring structures. (E) Quantification of the number of nuclei per osteoclast. (F) Quantification of the number of podosomes per indicated area in B. (G) Osteoclast height from WT and RAGE$^{-/-}$ cells was determined by confocal microscopy as the mean distance from the matrix surface to the apex of the basolateral membrane of single osteoclasts plated on glass and stained with phalloidin. **, $P < 0.01$, significant difference from WT (Student's *t* test).

osteoclasts, a process essential for osteoclast function (12). The defects in integrin signal transduction in RAGE$^{-/-}$ pre-OCs led us to examine F-actin structures in RAGE$^{-/-}$ osteoclasts cultured on glass by phalloidin staining. RAGE$^{-/-}$, TRAP-positive multinucleated cells showed membrane ruffles, contrasting with a belt of podosomes/actin rings along the peripheral membranes of WT osteoclasts (Fig. 5 A). In addition, loss of RAGE in BMMs resulted in a significantly reduced number of actin ring–containing cells (Figs. 5, A and D). Moreover, the average number of podosomes per unit area and the average number of nuclei per multinucleated cell were reduced in RAGE$^{-/-}$ osteoclasts (Figs. 5 A, B, E, and F). The latter situation is reminiscent of that seen in partially differentiated osteoclasts.

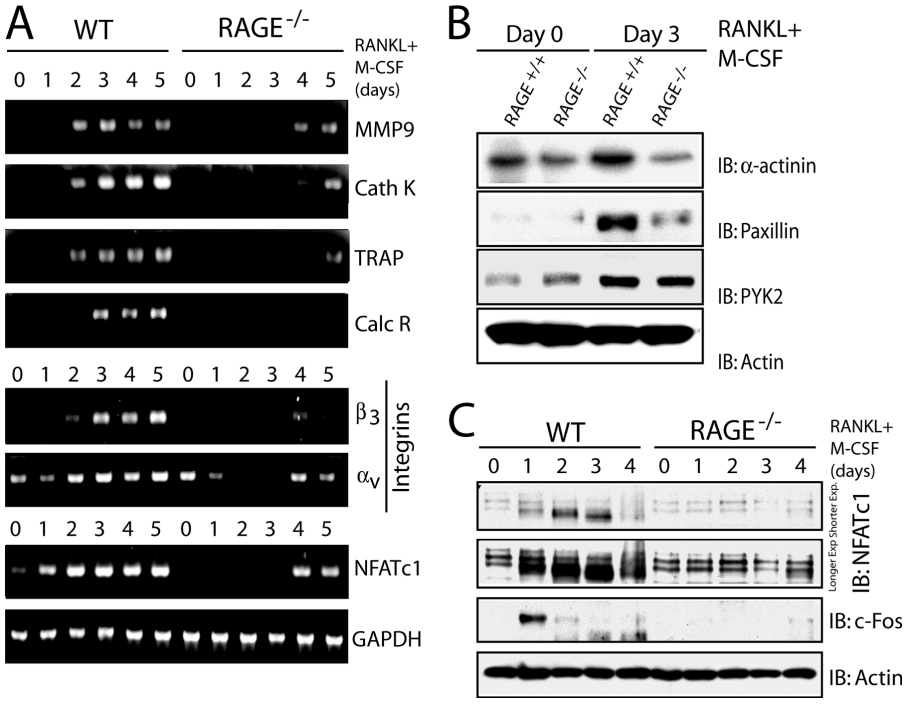


**Figure 6. Impaired osteoclast maturation and induction of NFATc1, integrins ($\alpha_v\beta_3$), α-actinin, and paxillin in RAGE$^{-/-}$ pre-OCs.** (A) RT-PCR analysis to assess expression of transcripts for MMP9, cathepsin K (Cath K), TRAP, calcitonin receptor (Calc R), integrins $\beta_3$ and $\alpha_v$, and NFATc1 in in vitro WT and RAGE$^{-/-}$ BMMs cultures in the presence of RANKL (100 ng/ml) and M-CSF (1%) for the indicated days. GAPDH was used as an internal control. (B) Western blot analysis of the expression of α-actinin, paxillin, PYK2, and actin in WT and RAGE$^{-/-}$ BMMs (day 0) and pre-OCs (day 3). (C) Western blot analysis of the expression of NFATc1, c-Fos, and actin in WT and RAGE$^{-/-}$ BMMs cultures in the presence of RANKL (100 ng/ml) and M-CSF (1%) for the indicated days.

To evaluate whether the inability of RAGE$^{-/-}$ osteoclasts to generate actin rings leads to nonpolarized and, hence, dysfunctional osteoclasts, we measured the distance between the basolateral membrane facing the marrow space and the ruffled border (osteoclast height), which is used as an index of osteoclast polarization (38). RAGE$^{-/-}$ osteoclasts showed significantly reduced height compared with WT osteoclasts (Fig. 5 G), indicating defective osteoclast polarization. These results suggest that disrupted actin cytoskeletal organization in RAGE$^{-/-}$ osteoclasts may be responsible for the morphologic and functional defects observed in vitro and in vivo.

To examine whether RAGE$^{-/-}$ osteoclasts have defects in terminal differentiation/maturation, we examined expression of osteoclastogenic markers (matrix metaloproteinase 9 [MMP9], cathepsin K, TRAP, and calcitonin receptor) in WT and RAGE$^{-/-}$ BMMs cultured with RANKL and M-CSF using RT-PCR analysis. Although transcripts encoding these markers were induced by day 2 in WT cultures, this event was delayed until day 4 in RAGE$^{-/-}$ cultures (Fig. 6 A). In addition, induction of the calcitonin receptor, a marker of mature osteoclasts, was completely abolished in RAGE$^{-/-}$ cultures for 5 d (Fig. 6 A), consistent with impaired osteoclast (OC) maturation. Collectively, these results implicate RAGE in osteoclastic actin cytoskeletal organization and suggest a role for RAGE in osteoclast maturation.

### Down-regulated expression of $\alpha_v\beta_3$, α-actinin, and paxillin in RAGE$^{-/-}$ pre-OCs

Defects in vitronectin integrin–induced signal transduction in RAGE$^{-/-}$ cells led us to address whether expression of $\alpha_v\beta_3$, integrins for VN, is altered in RAGE mutant cells. RT-PCR analysis demonstrated enhanced expression of $\alpha_v\beta_3$ in WT cultures during osteoclast differentiation (Fig. 6 A). However, this induction was delayed and reduced in RAGE$^{-/-}$ cultures (Fig. 6 A). In addition, podosome/actin ring-associated proteins, α-actinin, paxillin, and PYK2 were up-regulated in WT pre-OCs (day 3 in culture) (Fig. 6 B). Increased expression of paxillin and α-actinin, but not PYK2, was also inhibited in RAGE$^{-/-}$ pre-OCs (Fig. 6 B). Collectively, these results suggest a role of RAGE in the expression of $\alpha_v\beta_3$, α-actinin, and paxillin during osteoclast differentiation. Such RAGE-mediated expression of genes/proteins may be critical for regulation of actin cytoskeletal organization in pre-OCs.

### Inhibition of c-Fos and NFATc1 expression induced by RANKL and M-CSF in RAGE$^{-/-}$ pre-OCs

To further understand how RAGE regulates osteoclast maturation and function, we examined expression of transcriptional factors essential for osteoclastogenesis, including c-Fos and NFATc1 (39, 40). WT BMM cultures in the presence of

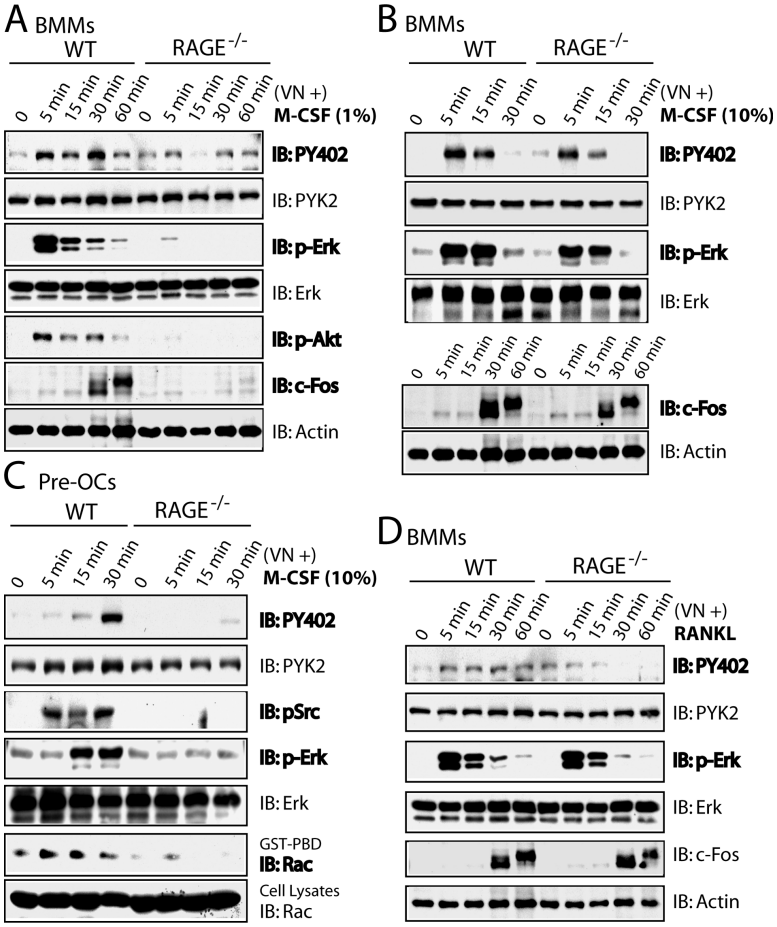


**Figure 7. Requirement of RAGE for the convergent signal transduction induced by $\alpha_v\beta_3$ integrin engagement and M-CSF.** BMMs (A, B, and D) and pre-OCs (C) from WT and RAGE$^{-/-}$ mice were lifted and replated on VN-coated dishes in the absence of serum. Adherent cells were treated with M-CSF at the indicated doses (A–C) or RANKL (D) for the indicated times and lysed. Equal amounts of total proteins were immunoblotted with the indicated antibodies, or pulled-down by GST-PBD to isolate GTP-bound Rac proteins (see Materials and methods).

M-CSF and RANKL showed an increase of c-Fos expression at day 1 and sustained induction of NFATc1 at both RNA and protein levels (Fig. 6, A and C). In contrast, such induction of c-Fos and NFATc1 was abolished in RAGE$^{-/-}$ cultures (Fig. 6, A and C). Note that immunoreactive NFATc1 migrated more rapidly in WT cells after exposure to RANKL and M-CSF (Fig. 6 C), probably caused by RANKL/M-CSF–induced activation of a calcium/calcineurin that caused dephosphorylation of NFATc1. This event was also abolished in RAGE$^{-/-}$ cells, indicating a role of RAGE in NFATc1 activation and induction (Fig. 6 C).

### Inhibition of convergent signal transduction induced by $\alpha_v\beta_3$ integrin engagement and M-CSF in RAGE$^{-/-}$ BMMs and pre-OCs

It has been reported that c-Fms and $\alpha_v\beta_3$ collaborate in osteoclastogenesis via shared activation of Erk signaling pathways critical for osteoclastic maturation (41, 42). Higher concentrations of M-CSF are capable of rescuing phenotypes associated with integrin $\beta_3$-deficient cells (42). Down-regulation of $\alpha_v\beta_3$ expression in RAGE$^{-/-}$ cells led us to examine whether RAGE$^{-/-}$ cells behave similarly to $\beta_3^{-/-}$ cells, whose phenotypes can be rescued by high dose of M-CSF treatment. Thus, we examined whether higher doses of M-CSF (e.g., 10%) could rescue signaling defects (e.g., PYK2 and Erk phosphorylation) in response to $\alpha_v\beta_3$ integrin engagement in RAGE$^{-/-}$ BMMs and pre-OCs. BMMs or day 3 pre-OCs generated from WT and RAGE$^{-/-}$ mice were lifted and replated on VN-coated dishes in the absence of serum. After treatment with M-CSF at lower (1%) or higher (10%) doses for different times, adherent cells were lysed and phosphorylation of PYK2, Src, and Erk1/2 and c-Fos activation/induction were examined. Although phosphorylation of PYK2 and Erk1/2 and c-Fos activation were induced by M-CSF at a low dose in WT BMMs, activation of these proteins was reduced or inhibited in RAGE$^{-/-}$ BMMs (Fig. 7 A), suggesting a defect of the convergent signaling by integrin engagement and M-CSF in RAGE$^{-/-}$ BMMs. Such signaling defects in BMMs could be rescued by treatment with a high dose of M-CSF; thus, M-CSF at 10% (a high dose) did induce PYK2

and Erk phosphorylation and c-Fos activation/induction (Fig. 7 B). In contrast, M-CSF, even at a high dose, failed to induce PYK2, Src, or Erk phosphorylation in RAGE$^{-/-}$ pre-OCs (Fig. 7 C). The latter observation suggests only a partial rescue of the RAGE$^{-/-}$ signaling defect by exposure to a high level of M-CSF in cells which have progressed down the osteoclast differentiation pathway. Consistent with these results, impaired osteoclast generation in RAGE$^{-/-}$ cultures could not be rescued by increasing M-CSF by amounts up to 10-fold (Fig. 8 A) or RANKL up to 4-fold (Fig. 8 B) compared with optimal doses for WT cultures. This situation contrasts with observations in integrin $\beta_3$ mutant cells, where higher concentrations of M-CSF do rescue the phenotype (42), but is reminiscent of that seen in TREM/DAP12 mutant cells (43).

In addition to PYK2, Src, and Erk, Rho family GTPases (e.g., Rac) known to be essential for actin cytoskeletal reorganization and cell spreading in OCs are also activated by M-CSF and integrin engagement (38). In view of impaired actin cytoskeletal organization and cell spreading observed in RAGE$^{-/-}$ pre-OCs, we assessed whether Rac activation by integrin engagement and M-CSF was inhibited. Indeed, deletion of the RAGE gene reduced Rac1 activation in response to M-CSF and integrin engagement compared with WT cells (Fig. 7 C). Collectively, these results suggest a requirement for RAGE in regulating the convergence of $\alpha_v\beta_3$ integrin- and M-CSF–mediated signals, which include activation of Rac, in addition to PYK2, Src, Erk, and c-Fos, in pre-OCs.

We also assessed whether RAGE is involved in the cross talk of the signaling transduction induced by RANKL and integrin engagement. To this end, BMMs generated from WT and RAGE$^{-/-}$ mice were lifted and replated on VN-coated dishes in the absence of serum. After treatment with RANKL for different times, adherent cells were lysed and phosphorylation of PYK2 and Erk1/2 and c-Fos activation/induction were examined. As shown in the Fig. 7 D, although integrin engagement appeared to enhance RANKL-induced Erk activation, the effect of RAGE in this event was minimal, suggesting that RAGE may not be involved in such cross talk between integrin and RANKL.

## DISCUSSION

RAGE, a multiligand receptor, contributes to the pathogenesis of multiple disorders, including diabetic complications, neuronal degeneration, and inflammatory disorders (32). In this study, we present evidence for a role of RAGE in regulating osteoclast maturation, function, and bone remodeling, which lead us to propose the model depicted in Fig. 9.

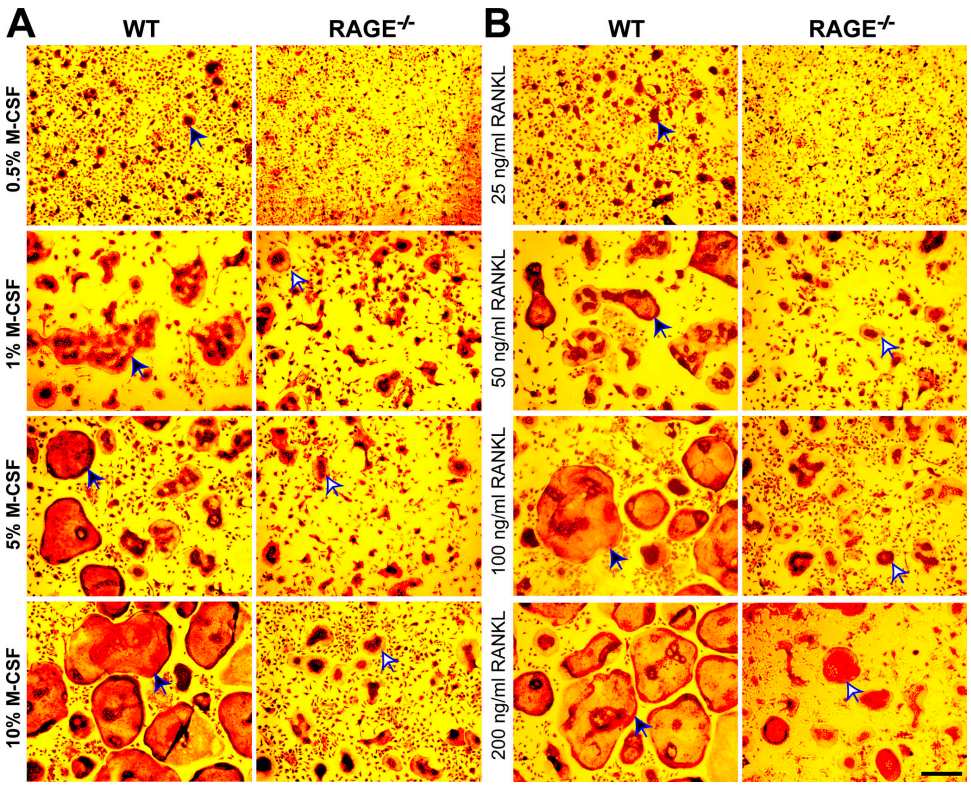


**Figure 8. Morphologic defects of RAGE$^{-/-}$ BMMs induced to differentiate in the presence of varying doses of M-CSF and RANKL.** BMMs from WT and RAGE$^{-/-}$ mice were cultured in the presence of the indicated concentrations of M-CSF and 200 ng/ml of RANKL (A) or in the presence of the indicated concentrations of RANKL and 5% of M-CSF (B). After 6 d of the treatment, TRAP staining was performed. The solid arrows in A and B indicate OCs in WT, and the open arrows indicate RAGE$^{-/-}$ OCs. Bar (applies to A and B), 50 μm.

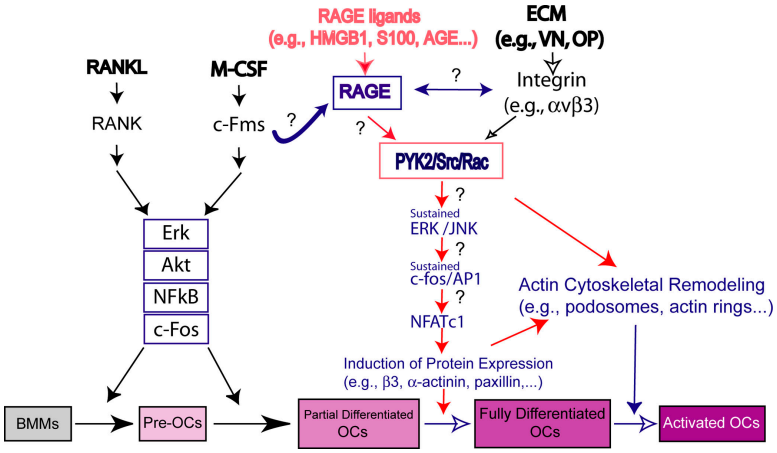


**Figure 9. A working hypothesis for RAGE-mediated regulation of osteoclast maturation and function.**

According to this model, RAGE, in response to its ligands, regulates convergent signals induced by integrin engagement and M-CSF that lead to actin cytoskeletal remodeling and osteoclastic maturation/activation (Fig. 9). Because of the dynamic nature of changes in the skeleton at young ages, different results might be obtained at later stages of bone development. However, based on the data presented here, we speculate that deletion of the RAGE gene might afford relative protection for the skeletal system in situations such as diabetes- or menopause-associated osteoclast activation.

Osteoclasts are tissue-specific macrophage polykaryon generated by the differentiation of monocyte/macrophage precursors at or near the bone surface. Close contact between stromal and bone marrow cells is essential for osteoclastogenesis in vivo, as stromal-derived factors, M-CSF and RANKL, activate receptors on BMMs, thereby stimulating osteoclast differentiation (1, 44). In addition to M-CSF and RANKL, Ig family receptors (e.g., TREM2) and integrin $\alpha_v\beta_3$ engagement play a crucial role in osteoclast terminal differentiation/maturation and function (8, 12, 45). Mice lacking TREM2 or $\alpha_v\beta_3$ show increased bone mass and develop osteosclerosis (7, 46). In this context, deletion of the gene for DAP12, a downstream mediator of TREM2 (7), or Src, a cytoplasmic tyrosine kinase whose activation depends on integrin engagement, results in mice with similar osteosclerotic phenotypes (16, 18, 20). In these mutant mice, osteoclast terminal differentiation/maturation is blunted in vitro (6, 7, 16, 18, 20). Moreover, actin cytoskeletal organization, e.g., actin ring and podosome formation, is disrupted in osteoclasts derived from these mutant animals (6, 7, 16, 18, 20, 43). Furthermore, the induction of NFATc1 by RANKL and M-CSF is abolished in TREM2/DAP12–deficient cells (5). In the current study, we demonstrate that RAGE$^{-/-}$ mice exhibit similar phenotypes to those observed in integrin $\beta_3$, Src, TREM2, and DAP12-deficient mice (46, 47), suggesting functional similarity of Ig family receptors, RAGE and TREM2, and implicating potential cross talk between RAGE and integrin $\alpha_v\beta_3$-mediated signaling pathways.

There is convergence of signaling downstream from c-Fms and $\alpha_v\beta_3$ integrins which contributes to osteoclast maturation and function (42). Thus, high doses of M-CSF can rescue the phenotypes observed in $\beta_3^{-/-}$ mice (42). However, morphologic abnormalities in RAGE$^{-/-}$ pre-OCs failed to be rescued by higher doses of M-CSF, suggesting a difference between RAGE$^{-/-}$ and $\beta_3^{-/-}$ mice. Moreover, sustained Erk activation is proposed to be a convergent signal consequent to engagement of c-Fms and $\alpha_v\beta_3$ integrins in osteoclast maturation (42). The latter event is inhibited in RAGE$^{-/-}$ pre-OCs, consistent with the observed inability of M-CSF to rescue RAGE$^{-/-}$ morphologic phenotypes and supporting a role for sustained Erk activation in osteoclast differentiation/maturation. Furthermore, serum M-CSF is increased in $\beta_3^{-/-}$ (42), but not in RAGE$^{-/-}$ mice (unpublished data), which is believed to play an important role in rescuing osteoclast differentiation in $\beta_3^{-/-}$ mice (42). Collectively, these observations implicate a role of RAGE in the convergent signaling mechanisms linking c-Fms and integrin $\alpha_v\beta_3$, and suggest that convergent downstream signals including activation of PYK2, Src, Rac, and Erk are altered in RAGE$^{-/-}$ pre-OCs. In this context, we speculate that PYK2/Src/Rac may be important convergent signals regulated by multiple receptors including integrins, c-Fms, and RAGE. This mechanism might be involved in sustained activation of MAPKs (Erk and JNK) and induction of transcription factors (c-Fos and NFATc1) (Fig. 9). This concept is consistent with the observation that integrin engagement appears to be a permissive factor for activation of PYK2, Src, and Rac by M-CSF, and that activation of PYK2, Src, or Rac is sufficient to stimulate Erk/JNK in different cells (48).

Mechanisms underlying RAGE-mediated regulation of integrin signaling remain to be delineated, though multiple pathways may be involved. We hypothesize that RAGE may regulate integrin signaling at the transcriptional level, at the cell surface (by possible direct association with integrins), and intracellularly. The observed decreased expression of integrins ($\alpha_v\beta_3$) in RAGE$^{-/-}$ pre-OCs supports a role for RAGE

in regulation of integrin expression at the transcriptional level, though the mechanism is unclear. We speculate that sustained Erk and c-Fos activation and induction of NFATc1 may have critical roles in this event. These observations do not exclude the possibility that RAGE might regulate integrin signaling via direct binding to integrins. In this context, endothelial RAGE has been shown to associate with $\beta_2$ integrins in leucocytes (29). Thus, it would be of interest to examine whether RAGE-bearing BMMs or osteoclasts can interact with the same cells (i.e., in cis) bearing $\beta_2$ integrins, thereby resulting in an autocrine regulatory loop.

In addition, we speculate that RAGE may be critical for PYK2 and sustained Erk activation by integrin and c-Fms engagement, events required for expression of integrin $\beta_3$, α-actinin, and paxillin during osteoclast maturation (Fig. 9). This notion is supported by previous reports that RAGE plays a crucial role in sustained Erk activation in multiple cell types (49, 50) and that sustained Erk activation is required for expression of $\beta_3$ (41). What are possible underlying mechanisms? Binding of ligands to RAGE on different cells such as endothelial cells, neurons, smooth muscle cells, or monocytes has been shown to activate a range of signaling pathways including Erk1/2 (p44/p42), p38 and JNK MAP kinases, rho GTPases, phosphoinositol 3-kinase, and the JAK/STAT pathway, as well as NF-κB signaling (32, 51). In addition, RAGE engagement can trigger generation of reactive oxygen species (ROS), at least in part via activation of NADPH oxidase (52–54). We speculate that RAGE-dependent ROS generation may underlie PYK2 and sustained Erk phosphorylation during osteoclast differentiation. In this context, it is relevant that ROS can be induced by M-CSF and RANKL in BMMs, and such ROS appear to be required for osteoclast actin ring formation and osteoclastic maturation and function (55–57). However, whether RAGE regulates integrin signaling through similar mechanisms remains to be determined.

In summary, we provide evidence for a contribution of RAGE to osteoclast maturation and function which is consistent with the receptor's emerging role in dendritic cell maturation/function (58, 59). These observations implicate RAGE more generally in the maturation of monocyte/macrophage lineage cells, an important cellular process for innate immunity and inflammatory responses. In addition, our results suggest that RAGE may function as a costimulatory receptor similar to other ITAM Ig family receptors (e.g., TREM2), thereby delivering essential signals for terminal osteoclastic differentiation, in concert with RANKL, M-CSF, and integrin-mediated signaling cascades (5, 7, 8, 39). Furthermore, our results suggest that RAGE may be an additional target for the design of therapeutic approaches to treat bone loss–related disorders.

## MATERIALS AND METHODS

**Reagents and animals.** Antibody specific to phospho-PYK2 (PY402) was purchased from Transduction Laboratories, Inc., and antibodies to phospho-Src (mAb PY416), phospho-Akt (P-Akt), Akt, phospho-Erk1/2 (p-Erk1/2), and Erk1/2 were from Cell Signaling. Monoclonal anti-$\alpha_v\beta_3$ and NFATc1 antibodies were purchased from Abcam, Inc. and BD PharMingen, respectively. The c-Fos polyclonal antibody was from Santa Cruz Biotechnology, Inc. RAGE antibody (mAb) was purchased from Chemicon, and RAGE polyclonal antibody was generated by GST-RAGE COOH-terminal fusion protein. VN was obtained from Sigma-Aldrich. 1α,25-dihydroxyvitamin $D_3$ (1α, 25$[OH]_2D_3$) and collagenase were obtained from Wako Chemicals, and dispase was purchased from Roche. Murine M-CSF was obtained from R&D Systems. Recombinant GST-RANKL was generated and purified as described previously (60). $RAGE^{-/-}$ mice described previously (37) were crossed into C57BL/6 genetic background. Age-matched C57BL/6 WT mice were used as controls. RAGE mutation was confirmed by the expression of GFP, an indicator of the Cre expression in the mice (37), RT-PCR for its mRNA expression, and Western blot analysis. All experimental procedures were approved by the Animal Subjects Committee at the Medical College of Georgia, according to U.S. National Institutes of Health guidelines.

**In vitro osteoclastogenesis using whole bone marrow cells.** Bone marrow cultures were prepared using previously described methods with modifications (13). In brief, the bone marrow was flushed from femurs and tibiae with ice-cold α-MEM (GIBCO BRL). Cells were collected, pelleted, and resuspended in α-MEM supplemented with 10% FBS (Hyclone) and cultured in 6-well plates at a density of $2.5 \times 10^6/cm^2$ for 7 d in the presence of $2.5 \times 10^{-8}$ M 1,25$(OH)_2D_3$. At day 4 of culture, 90% of the medium with 1,25$(OH)_2D_3$ was replaced. At day 8, cultures were fixed and stained for TRAP using the Leukocyte Acid Phosphatase kit (Sigma-Aldrich).

**In vitro osteoclastogenesis using purified BMMs.** Mouse BMMs, pre-OCs, and osteoclasts were generated as described (13). In brief, whole bone marrow cells were flushed from long bones of 4–6-wk-old WT or $RAGE^{-/-}$ mice and plated on 100-mm tissue culture plates in α-MEM containing 10% FBS and 10 ng/ml recombinant M-CSF (R&D Systems). Cells were incubated at 37°C with 5% $CO_2$ overnight. Nonadherent cells were harvested and subjected to Ficoll-Hypaque gradient centrifugation for purification of BMMs. Isolated BMMs were then cultured in α-MEM containing 10% FBS plus 10 ng/ml recombinant M-CSF. To generate pre-OCs, BMMs were cultured in α-MEM containing 10% FBS in the presence of 10 ng/ml recombinant M-CSF and 100 ng/ml recombinant GST-RANKL for 2–3 d. To generate mature OCs, $5 \times 10^4$ BMMs were plated in one well of a 24-well plate in α-MEM containing 10% FBS in the presence of 10 ng/ml recombinant M-CSF and 100 ng/ml recombinant GST-RANKL. Mature osteoclasts (multinucleated, large, spread cells) began to form at day 4 of culture. The identity of osteoclasts was confirmed by TRAP staining.

**In vitro resorption assay of cultured OCs.** BMMs were replated in 16-well BD BioCoat Osteologic slides (BD Biosciences), which are coated with inorganic hydroxyapatite matrix, in the presence of M-CSF (2%) and RANKL (100 ng/ml). After 8 d, cells were washed and stained with Von Kossa. Resorption pits were analyzed using National Institutes of Health Image software.

**In vivo bone resorption assay.** Mouse bone resorption activity was determined by measuring serum Pyd concentration using METRA Serum PYD EIA kit (QUIDEL Corporation) according to the manufacturer's instructions. In brief, filtered serum samples (25 μl) were incubated with 75 μl Pyd antibody and reagent overnight at 4°C in the dark. After washing three times, samples were incubated with enzyme conjugate for 60 min at room temperature. Substrate solution (150 μl) was added to samples after washing and incubated at room temperature for 40 min. The reaction was stopped, and the OD was measured at 405 nm. OD was then converted to Pyd concentration using a standard curve. All the samples were measured in duplicate, and values were subjected to statistical analysis.

**Radiographic, densitometric, and μCT analysis of bone mass.** A dual energy x-ray (DEXA) PIXImus densitometer was used to measure bone mineral density of whole bone mass from 4-wk-old mice. In addition, long bones (e.g., femurs and tibia) and spines were isolated from mice (4−6 wk old) and subjected to radiographic analysis using x-ray and μCT analysis. x-ray

projection images were acquired from a custom in-house μCT system consisting of a microfocal x-ray source, a 4-axis manipulator (Danaher Motion) and an amorphorous silicon flat panel image (Paxscan 4030; Varian Medical Systems). For a given examination, 570 projection images were acquired over 360° rotation with an exposure time of 11.2 s for each image. The x-ray source was configured with a 15-μm spot, 60 kV tube voltage, and 0.15 mA tube current. The x-rays were filtered through 0.4 mm AL and 1.3 mm Teflon. The samples were positioned to produce a geometric magnification of 8.5 resulting in a reconstruction voxel size of 15 μm. Three-dimensional reconstruction was performed by Lawrence Livermore National Laboratory software using the Feldkamp cone-beam algorithm. Three-dimensional surfacing was performed using IDL software (Research Systems, Inc.). Bone volume (BV) to tissue volume (TV) ratio measurements were generated by first segmenting the calcified bone tissue with an appropriate threshold level and then dividing the number of these segmented bone tissue voxels by the number of voxels enclosed by the same segmentation threshold level.

**Bone histomorphometric analysis.** Mouse tibia and femurs were fixed overnight in 10% buffered formalin, decalcified in 14% EDTA, embedded in paraffin, sectioned, and stained for TRAP with a methyl green counterstain. Bone histomorphometric perimeters were determined by measuring the areas situated at least 0.5 mm from the growth plate, excluding the primary spongiosa and trabeculae connected to the cortical bone.

**Immunofluorescence.** WT and RAGE$^{-/-}$ osteoclasts cultured on glass were fixed and stained with Texas red–phalloidin as previously described (13). To measure osteoclast height, the distance between the basolateral membrane (top of the cell) and the ruffled border (bottom of the cell, facing the matrix) was determined using confocal microscopy.

**Western blot analysis.** BMMs or pre-OCs were cultured and then starved overnight in serum-free media. Cells were lifted and replated on VN for the indicated times. For some experiments, cells were further stimulated with 5 ng/ml M-CSF followed by lysis in RIPA buffer described previously (61). Lysates were subjected to SDS-PAGE and immunoblotting analysis using the indicated antibodies.

**RT-PCR analysis.** Total RNA was prepared from BMMs, pre-OCs, and osteoclasts derived from WT and RAGE$^{-/-}$ mice using Trizol (Invitrogen). These cells were generated as described (see In vitro osteoclastogenesis using purified BMMs), at day 0 (BMMs), day 2 (pre-OCs), and day 4 (osteoclasts) in culture in the presence of M-CSF and RANKL. cDNAs were synthesized from 2 μg of total RNA using SuperScript III First Strand Synthesis System (Invitrogen) in a volume of 20 μl. The reaction mixture was adjusted to 100 μl with distilled water. One microliter of cDNA was amplified with the specific primers indicated by PCR. The PCR product was separated on a 1.5% agarose gel and visualized by ethidium bromide staining. The following primers were used: integrin $\alpha_v$, 5′-AACATCACCTGGGGCATTCA-3′ and 5′-CGTCAGTGTGGGCGAAGTAAA-3′; integrin $\beta_3$, 5′-TTACCCCGTGGACATCTACTA-3′ and 5′-AGTCTTCCATCCAGGGCAATA-3′; calcitonin receptor, 5′-CATTCCTGTACTTGGTTGGC-3′ and 5′-AGCAATCGACAAGGAGTGAC-3′; MMP9, 5′-CCTGTGTGTTCCCGTTCATCT-3′ and 5′-CGCTGGAATGATCTAAGCCCA-3′; TRAP, 5′-ACAGCCCCCCACTCCCACCCT-3′ and 3′-TCAGGGTCTGGGTCTCCTTGG-5′; cathepsin K, 5′-GGAAGAAGACTCACCAGAAGC-3′ and 3′-GTCATATAGCCGCCTCCACAG-5′; NFATc1, 5′-TGCTCCTCCTCCTGCTGCTC-3′ and 5′-CGTCTTCCACCTCCACGTCG-3′, and GAPDH, 5′-TGAAGGTCGGTGTGAACGGATTTGGC-3′ and 3′-CATGTAGGCCATGAGGTCCACCAC-5′.

**Rac activation assay.** Rac activation (GTP-bound Rac) was determined by its specific binding to the p21-binding domain of PAK1 (GST-PBT) as described previously (61). In brief, cell lysates from pre-OCs cultured in VN-coated dishes and treated with M-CSF (10%) for indicated time were incubated with GST-PBD fusion protein (5 μg, conjugated with glutathione-agarose beads) for 60 min at 4°C. Bound Rac was analyzed by Western blot analysis using anti-Rac antibodies. Whole cell lysates were also analyzed for the expression of endogenous Rac for normalization.

**Statistical analysis.** Data were analyzed using an unpaired two-tailed Student's *t* test and are expressed as the mean plus/minus SEM. p values less than 0.05 were considered significant.

We are grateful to Dr. Lih-Fen Lue (Sun Health Research Institute, Sun City, AZ) for providing reagents. We also thank Drs. Jian-Xin Xie and Xin-Ming Shi (Medical College of Georgia) for their assistance with RT-PCR.

This study was supported in part by grants from the National Institutes of Health (AR47830 to X. Feng; NS40480, NS045710, and NS44521 for L. Mei; AR48120 and GM63861 to W-C. Xiong) and grants from the Deutsche Forschungsgemeinschaft (SFB 405 to P.P. Nawroth).

W.-C. Xiong, D.M. Stern, L. Mei, and Z. Zhou are co-inventors on one or more patent applications involving the RAGE technology.

The authors have no other conflicting financial interests.

**Submitted: 29 September 2005**
**Accepted: 13 March 2006**

## REFERENCES

1. Boyle, W.J., W.S. Simonet, and D.L. Lacey. 2003. Osteoclast differentiation and activation. *Nature*. 423:337–342.
2. Tanaka, S., N. Takahashi, N. Udagawa, T. Tamura, T. Akatsu, E.R. Stanley, T. Kurokawa, and T. Suda. 1993. Macrophage colony-stimulating factor is indispensable for both proliferation and differentiation of osteoclast progenitors. *J. Clin. Invest*. 91:257–263.
3. Yasuda, H., N. Shima, N. Nakagawa, K. Yamaguchi, M. Kinosaki, S. Mochizuki, A. Tomoyasu, K. Yano, M. Goto, A. Murakami, et al. 1998. Osteoclast differentiation factor is a ligand for osteoprotegerin/osteoclastogenesis-inhibitory factor and is identical to TRANCE/RANKL. *Proc. Natl. Acad. Sci. USA*. 95:3597–3602.
4. Lacey, D.L., E. Timms, H.L. Tan, M.J. Kelley, C.R. Dunstan, T. Burgess, R. Elliott, A. Colombero, G. Elliott, S. Scully, et al. 1998. Osteoprotegerin ligand is a cytokine that regulates osteoclast differentiation and activation. *Cell*. 93:165–176.
5. Koga, T., M. Inui, K. Inoue, S. Kim, A. Suematsu, E. Kobayashi, T. Iwata, H. Ohnishi, T. Matozaki, T. Kodama, et al. 2004. Costimulatory signals mediated by the ITAM motif cooperate with RANKL for bone homeostasis. *Nature*. 428:758–763.
6. Cella, M., C. Buonsanti, C. Strader, T. Kondo, A. Salmaggi, and M. Colonna. 2003. Impaired differentiation of osteoclasts in TREM-2–deficient individuals. *J. Exp. Med*. 198:645–651.
7. Paloneva, J., J. Mandelin, A. Kiialainen, T. Bohling, J. Prudlo, P. Hakola, M. Haltia, Y.T. Konttinen, and L. Peltonen. 2003. DAP12/TREM2 deficiency results in impaired osteoclast differentiation and osteoporotic features. *J. Exp. Med*. 198:669–675.
8. Colonna, M. 2003. TREMs in the immune system and beyond. *Nat. Rev. Immunol*. 3:445–453.
9. Yagi, M., T. Miyamoto, Y. Sawatani, K. Iwamoto, N. Hosogane, N. Fujita, K. Morita, K. Ninomiya, T. Suzuki, K. Miyamoto, et al. 2005. DC-STAMP is essential for cell–cell fusion in osteoclasts and foreign body giant cells. *J. Exp. Med*. 202:345–351.
10. Kim, N., Y. Kadono, M. Takami, J. Lee, S.H. Lee, F. Okada, J.H. Kim, T. Kobayashi, P.R. Odgren, H. Nakano, et al. 2005. Osteoclast differentiation independent of the TRANCE-RANK-TRAF6 axis. *J. Exp. Med*. 202:589–595.
11. Kim, N., M. Takami, J. Rho, R. Josien, and Y. Choi. 2002. A novel member of the leukocyte receptor complex regulates osteoclast differentiation. *J. Exp. Med*. 195:201–209.
12. Teitelbaum, S.L. 2000. Osteoclasts, integrins, and osteoporosis. *J. Bone Miner. Metab*. 18:344–349.
13. Wang, Q., Y. Xie, Q.S. Du, X.J. Wu, X. Feng, L. Mei, J.M. McDonald, and W.C. Xiong. 2003. Regulation of the formation of osteoclastic actin rings by proline-rich tyrosine kinase 2 interacting with gelsolin. *J. Cell Biol*. 160:565–575.

14. Chellaiah, M., N. Kizer, M. Silva, U. Alvarez, D. Kwiatkowski, and K.A. Hruska. 2000. Gelsolin deficiency blocks podosome assembly and produces increased bone mass and strength. *J. Cell Biol.* 148:665–678.
15. Marchisio, P.C., D. Cirillo, L. Naldini, M.V. Primavera, A. Teti, and A. Zambonin-Zallone. 1984. Cell-substratum interaction of cultured avian osteoclasts is mediated by specific adhesion structures. *J. Cell Biol.* 99:1696–1705.
16. Boyce, B.F., T. Yoneda, C. Lowe, P. Soriano, and G.R. Mundy. 1992. Requirement of pp60c-src expression for osteoclasts to form ruffled borders and resorb bone in mice. *J. Clin. Invest.* 90:1622–1627.
17. Pfaff, M., and P. Jurdic. 2001. Podosomes in osteoclast-like cells: structural analysis and cooperative roles of paxillin, proline-rich tyrosine kinase 2 (Pyk2) and integrin alphaVbeta 3. *J. Cell Sci.* 114: 2775–2786.
18. Duong, L.T., P.T. Lakkakorpi, I. Nakamura, M. Machwate, R.M. Nagy, and G.A. Rodan. 1998. PYK2 in osteoclasts is an adhesion kinase, localized in the sealing zone, activated by ligation of alpha(v)beta3 integrin, and phosphorylated by src kinase. *J. Clin. Invest.* 102:881–892.
19. Nakamura, I., E. Jimi, L.T. Duong, T. Sasaki, N. Takahashi, G.A. Rodan, and T. Suda. 1998. Tyrosine phosphorylation of p130Cas is involved in actin organization in osteoclasts. *J. Biol. Chem.* 273:11144–11149.
20. Sanjay, A., A. Houghton, L. Neff, E. DiDomenico, C. Bardelay, E. Antoine, J. Levy, J. Gailit, D. Bowtell, W.C. Horne, and R. Baron. 2001. Cbl associates with Pyk2 and Src to regulate Src kinase activity, alpha(v)beta(3) integrin-mediated signaling, cell adhesion, and osteoclast motility. *J. Cell Biol.* 152:181–195.
21. Chiusaroli, R., A. Sanjay, K. Henriksen, M.T. Engsig, W.C. Horne, H. Gu, and R. Baron. 2003. Deletion of the gene encoding c-Cbl alters the ability of osteoclasts to migrate, delaying resorption and ossification of cartilage during the development of long bones. *Dev. Biol.* 261:537–547.
22. Nakamura, I., T. Sasaki, S. Tanaka, N. Takahashi, E. Jimi, T. Kurokawa, Y. Kita, S. Ihara, T. Suda, and Y. Fukui. 1997. Phosphatidylinositol-3 kinase is involved in ruffled border formation in osteoclasts. *J. Cell. Physiol.* 172:230–239.
23. Chellaiah, M.A., N. Soga, S. Swanson, S. McAllister, U. Alvarez, D. Wang, S.F. Dowdy, and K.A. Hruska. 2000. Rho-A is critical for osteoclast podosome organization, motility, and bone resorption. *J. Biol. Chem.* 275:11993–12002.
24. Brownlee, M. 2000. Negative consequences of glycation. *Metabolism.* 49:9–13.
25. Nawroth, P., A. Bierhaus, M. Marrero, H. Yamamoto, and D.M. Stern. 2005. Atherosclerosis and restenosis: is there a role for RAGE? *Curr. Diab. Rep.* 5:11–16.
26. Lue, L.F., S.D. Yan, D.M. Stern, and D.G. Walker. 2005. Preventing activation of receptor for advanced glycation endproducts in Alzheimer's disease. *Curr. Drug Targets CNS Neurol. Disord.* 4:249–266.
27. Bierhaus, A., P.M. Humpert, D.M. Stern, B. Arnold, and P.P. Nawroth. 2005. Advanced glycation end product receptor-mediated cellular dysfunction. *Ann. N. Y. Acad. Sci.* 1043:676–680.
28. Bierhaus, A., S. Schiekofer, M. Schwaninger, M. Andrassy, P.M. Humpert, J. Chen, M. Hong, T. Luther, T. Henle, I. Kloting, et al. 2001. Diabetes-associated sustained activation of the transcription factor nuclear factor-kappaB. *Diabetes.* 50:2792–2808.
29. Chavakis, T., A. Bierhaus, N. Al-Fakhri, D. Schneider, S. Witte, T. Linn, M. Nagashima, J. Morser, B. Arnold, K.T. Preissner, and P.P. Nawroth. 2003. The pattern recognition receptor (RAGE) is a counter-receptor for leukocyte integrins: a novel pathway for inflammatory cell recruitment. *J. Exp. Med.* 198:1507–1515.
30. Taguchi, A., D.C. Blood, G. del Toro, A. Canet, D.C. Lee, W. Qu, N. Tanji, Y. Lu, E. Lalla, C. Fu, et al. 2000. Blockade of RAGE-amphoterin signalling suppresses tumour growth and metastases. *Nature.* 405:354–360.
31. Lotze, M.T., and K.J. Tracey. 2005. High-mobility group box 1 protein (HMGB1): nuclear weapon in the immune arsenal. *Nat. Rev. Immunol.* 5:331–342.
32. Chavakis, T., A. Bierhaus, and P.P. Nawroth. 2004. RAGE (receptor for advanced glycation end products): a central player in the inflammatory response. *Microbes Infect.* 6:1219–1225.
33. Basta, G., G. Lazzerini, M. Massaro, T. Simoncini, P. Tanganelli, C. Fu, T. Kislinger, D.M. Stern, A.M. Schmidt, and R. De Caterina. 2002. Advanced glycation end products activate endothelium through signal-transduction receptor RAGE: a mechanism for amplification of inflammatory responses. *Circulation.* 105:816–822.
34. Boulanger, E., M.P. Wautier, J.L. Wautier, B. Boval, Y. Panis, N. Wernert, P.M. Danze, and P. Dequiedt. 2002. AGEs bind to mesothelial cells via RAGE and stimulate VCAM-1 expression. *Kidney Int.* 61:148–156.
35. Treutiger, C.J., G.E. Mullins, A.S. Johansson, A. Rouhiainen, H.M. Rauvala, H. Erlandsson-Harris, U. Andersson, H. Yang, K.J. Tracey, J. Andersson, and J.E. Palmblad. 2003. High mobility group 1 B-box mediates activation of human endothelium. *J. Intern. Med.* 254: 375–385.
36. Liliensiek, B., M.A. Weigand, A. Bierhaus, W. Nicklas, M. Kasper, S. Hofer, J. Plachky, H.J. Grone, F.C. Kurschus, A.M. Schmidt, et al. 2004. Receptor for advanced glycation end products (RAGE) regulates sepsis but not the adaptive immune response. *J. Clin. Invest.* 113:1641–1650.
37. Constien, R., A. Forde, B. Liliensiek, H.J. Grone, P. Nawroth, G. Hammerling, and B. Arnold. 2001. Characterization of a novel EGFP reporter mouse to monitor Cre recombination as demonstrated by a Tie2 Cre mouse line. *Genesis.* 30:36–44.
38. Faccio, R., S.L. Teitelbaum, K. Fujikawa, J. Chappel, A. Zallone, V.L. Tybulewicz, F.P. Ross, and W. Swat. 2005. Vav3 regulates osteoclast function and bone mass. *Nat. Med.* 11:284–290.
39. Takayanagi, H. 2005. Mechanistic insight into osteoclast differentiation in osteoimmunology. *J. Mol. Med.* 83:170–179.
40. Matsuo, K., and N. Irie. 2005. Transcription factors in osteoclast differentiation. *Nippon Rinsho.* 63:1541–1546.
41. Woods, D., H. Cherwinski, E. Venetsanakos, A. Bhat, S. Gysin, M. Humbert, P.F. Bray, V.L. Saylor, and M. McMahon. 2001. Induction of beta3-integrin gene expression by sustained activation of the Ras-regulated Raf-MEK-extracellular signal-regulated kinase signaling pathway. *Mol. Cell. Biol.* 21:3192–3205.
42. Faccio, R., S. Takeshita, A. Zallone, F.P. Ross, and S.L. Teitelbaum. 2003. c-Fms and the alphavbeta3 integrin collaborate during osteoclast differentiation. *J. Clin. Invest.* 111:749–758.
43. Faccio, R., W. Zou, G. Colaianni, S.L. Teitelbaum, and F.P. Ross. 2003. High dose M-CSF partially rescues the Dap12−/− osteoclast phenotype. *J. Cell. Biochem.* 90:871–883.
44. Xiong, W.C., and X. Feng. 2003. PYK2 and FAK in osteoclasts. *Front. Biosci.* 8:d1219–d1226.
45. Teitelbaum, S.L., and F.P. Ross. 2003. Genetic regulation of osteoclast development and function. *Nat. Rev. Genet.* 4:638–649.
46. McHugh, K.P., K. Hodivala-Dilke, M.H. Zheng, N. Namba, J. Lam, D. Novack, X. Feng, F.P. Ross, R.O. Hynes, and S.L. Teitelbaum. 2000. Mice lacking beta3 integrins are osteosclerotic because of dysfunctional osteoclasts. *J. Clin. Invest.* 105:433–440.
47. Berry, V., H. Rathod, L.B. Pulman, and H.K. Datta. 1994. Immunofluorescent evidence for the abundance of focal adhesion kinase in the human and avian osteoclasts and its down regulation by calcitonin. *J. Endocrinol.* 141:R11–R15.
48. Sekimoto, H., J. Eipper-Mains, S. Pond-Tor, and C.M. Boney. 2005. (alpha)v(beta)3 integrins and Pyk2 mediate insulin-like growth factor I activation of Src and mitogen-activated protein kinase in 3T3-L1 cells. *Mol. Endocrinol.* 19:1859–1867.
49. Ishihara, K., K. Tsutsumi, S. Kawane, M. Nakajima, and T. Kasaoka. 2003. The receptor for advanced glycation end-products (RAGE) directly binds to ERK by a D-domain-like docking site. *FEBS Lett.* 550:107–113.
50. McDonald, D.R., M.E. Bamberger, C.K. Combs, and G.E. Landreth. 1998. beta-Amyloid fibrils activate parallel mitogen-activated protein kinase pathways in microglia and THP1 monocytes. *J. Neurosci.* 18:4451–4460.
51. Bucciarelli, L.G., T. Wendt, L. Rong, E. Lalla, M.A. Hofmann, M.T. Goova, A. Taguchi, S.F. Yan, S.D. Yan, D.M. Stern, and A.M. Schmidt. 2002. RAGE is a multiligand receptor of the immunoglobulin superfamily: implications for homeostasis and chronic disease. *Cell. Mol. Life Sci.* 59:1117–1128.

52. Wautier, M.P., O. Chappey, S. Corda, D.M. Stern, A.M. Schmidt, and J.L. Wautier. 2001. Activation of NADPH oxidase by AGE links oxidant stress to altered gene expression via RAGE. *Am. J. Physiol. Endocrinol. Metab.* 280:E685–E694.
53. Basta, G., G. Lazzerini, S. Del Turco, G.M. Ratto, A.M. Schmidt, and R. De Caterina. 2005. At least 2 distinct pathways generating reactive oxygen species mediate vascular cell adhesion molecule-1 induction by advanced glycation end products. *Arterioscler. Thromb. Vasc. Biol.* 25:1401–1407.
54. Mukherjee, T.K., S. Mukhopadhyay, and J.R. Hoidal. 2005. The role of reactive oxygen species in TNFalpha-dependent expression of the receptor for advanced glycation end products in human umbilical vein endothelial cells. *Biochim. Biophys. Acta.* 1744:213–223.
55. Lee, N.K., Y.G. Choi, J.Y. Baik, S.Y. Han, D.W. Jeong, Y.S. Bae, N. Kim, and S.Y. Lee. 2005. A crucial role for reactive oxygen species in RANKL-induced osteoclast differentiation. *Blood.* 106:852–859.
56. Ha, H., H.B. Kwak, S.W. Lee, H.M. Jin, H.M. Kim, H.H. Kim, and Z.H. Lee. 2004. Reactive oxygen species mediate RANK signaling in osteoclasts. *Exp. Cell Res.* 301:119–127.
57. Lean, J.M., J.T. Davies, K. Fuller, C.J. Jagger, B. Kirstein, G.A. Partington, Z.L. Urry, and T.J. Chambers. 2003. A crucial role for thiol antioxidants in estrogen-deficiency bone loss. *J. Clin. Invest.* 112:915–923.
58. Dumitriu, I.E., P. Baruah, M.E. Bianchi, A.A. Manfredi, and P. Rovere-Querini. 2005. Requirement of HMGB1 and RAGE for the maturation of human plasmacytoid dendritic cells. *Eur. J. Immunol.* 35:2184–2190.
59. Dumitriu, I.E., P. Baruah, B. Valentinis, R.E. Voll, M. Herrmann, P.P. Nawroth, B. Arnold, M.E. Bianchi, A.A. Manfredi, and P. Rovere-Querini. 2005. Release of high mobility group box 1 by dendritic cells controls T cell activation via the receptor for advanced glycation end products. *J. Immunol.* 174:7506–7515.
60. Lam, J., S. Takeshita, J.E. Barker, O. Kanagawa, F.P. Ross, and S.L. Teitelbaum. 2000. TNF-alpha induces osteoclastogenesis by direct stimulation of macrophages exposed to permissive levels of RANK ligand. *J. Clin. Invest.* 106:1481–1488.
61. Ren, X.R., Q.S. Du, Y.Z. Huang, S.Z. Ao, L. Mei, and W.C. Xiong. 2001. Regulation of CDC42 GTPase by proline-rich tyrosine kinase 2 interacting with PSGAP, a novel pleckstrin homology and Src homology 3 domain containing rhoGAP protein. *J. Cell Biol.* 152:971–984.